Zonally varying ITCZs in a Matsuno–Gill-type model with an idealized Bjerknes feedback

Ori Adam[1]

Key Points.

- Concurrent single and double ITCZs emerge in the limit of strong mechanical damping
- An idealized Bjerknes feedback produces an equatorial cold tongue
- The zonal orientation of the double ITCZs varies with the width of the equatorial cold tongue

Abstract. In the present climate, tropical rain bands exhibit a bifurcated pattern, continuously forming along single intertropical convergence zones (ITCZs) in some regions, and along double ITCZs that straddle the equator in other regions. This bifurcated ITCZ pattern is studied in a Matsuno–Gill-type model forced by relaxation to zonally asymmetric surface pressure. The model includes an idealized Bjerknes feedback which couples surface winds and sea surface temperatures (SSTs) via oceanic Ekman balance. Consistent with observations, solutions in the limit of strong damping are explored. Two ITCZ bifurcation mechanisms are identified. First, in the viscous limit, ITCZs form along negative anomalies of the local Rossby number, which tend to occur near the equator for equatorial low pressure and off the equator for equatorial high pressure; this leads to a single ITCZ in the rising branch of zonal overturning circulations and a double ITCZ that straddles the equator in the descending branch. Second, near the equator, ocean upwelling produces a cold tongue with increased surface pressure, which reduces vertical winds and can lead to precipitation peaks that straddle the equator in regions of equatorial ascent. Consistent with observations, the cold tongue intensifies with increasing zonal SST gradients, and its base widens with weakened poleward SST gradients, modulating the zonal orientation of the ITCZs on either side of the cold tongue. Analytic approximate solutions in the viscous limit capture the emergence of the bifurcated ITCZ pattern, as well as the dependence of the bifurcated ITCZ pattern on zonal and poleward SST gradients

1. Introduction

Tropical rain bands lie along near-surface convergence zones where the lower branches of the meridional overturning circulation intersect [*Xie*, 2004; *Schneider et al.*, 2014]. In the present climate, tropical rain bands exhibit a bifurcated pattern, continuously forming along single intertropical convergence zones (ITCZs) in some regions, and along double ITCZs that straddle the equator in other regions [e.g., *Zhang*, 2001]. Since the tropical overturning circulations in regions dominated by single and double ITCZs are inextricably linked, a theory of the zonally varying tropical rain belt requires consideration of the bifurcated pattern (i.e., concurrent single and double ITCZs) as a whole. The goal of this study is to gain a conceptual understanding of the bifurcated ITCZ pattern by revisiting classical Matsuno–Gill-type models of the tropics [*Matsuno*, 1966; *Gill*, 1980]. It is shown that these models shed light on the origin of the bifurcated ITCZ pattern and capture some of its key features.

Variants of the bifurcated ITCZ pattern exist in the present tropical climate on timescales of days or longer: daily states of the ITCZ in the eastern Pacific vary between single and double ITCZs that straddle the equator [*Haffke et al.*, 2016], with increased occurrence of double-ITCZ states during boreal spring and during La Niña episodes [*Zhang*, 2001; *Gu et al.*, 2005; *Bischoff and Schneider*, 2016; *Adam et al.*, 2016]; infrequent seasonal occurrences of double-ITCZ states are observed over the Indian Ocean and central Pacific [e.g., *Zhang*, 2001]; a regional bifurcation from a single ITCZ in the Indian Ocean to a south Pacific convergence zone (SPCZ) and a Pacific ITCZ north of the equator is observed year-round [e.g., *Adam et al.*, 2016]. Additionally, modern climate models tend to have more pronounced double ITCZs in the Pacific than is observed [e.g., *Lin*, 2007]. The precipitation response to greenhouse-induced global warming in these models also shows a bifurcated pattern with double precipitation peaks that straddle the equator in the Pacific, and a single peak elsewhere [e.g., *Held and Soden*, 2006; *Bony et al.*, 2013]. Yet, despite the prevalence of the bifurcated ITCZ pattern in the mean tropical climate and in perturbations of the tropical climate, a theory of the origin of this pattern does not exist.

In the zonal mean, the position of the ITCZ is dominated by inter-hemispheric differential heating, which, to first order, is controlled by the radiative budget at the top of the atmosphere [for a review see *Schneider et al.*, 2014]. In contrast, zonally asymmetric ITCZ variations are dominated by the complex nature of the zonally-asymmetric tropical dynamics and energy balance [*Adam et al.*, 2016; *Boos and Korty*, 2016]. In particular, a major obstacle to a theoretical understanding of ITCZ dynamics is the coupling of marine ITCZs and their associated atmospheric circulations, with the underlying sea surface temperatures (SSTs) and their associated oceanic circulations. This obstacle is addressed

[1]The Hebrew University, Jerusalem, Israel.

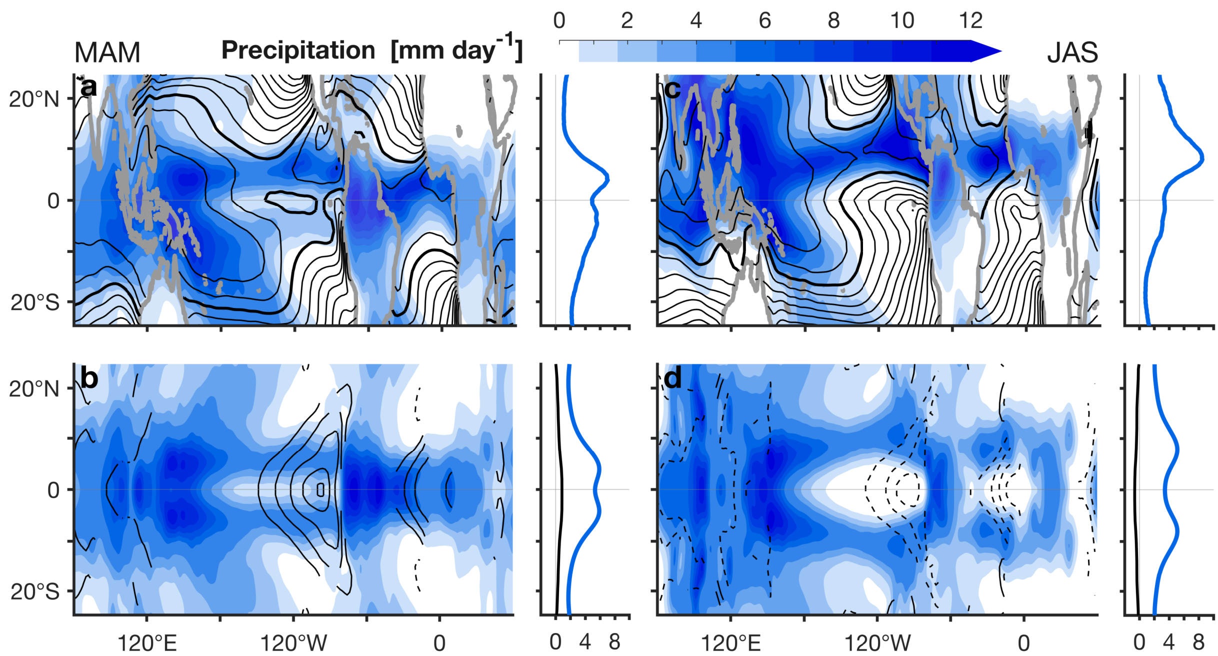

Figure 1. The tropical precipitation (blue) and the SST (black contours) during Mar–May (**a**,**b**) and Jul–Sep (**c**,**d**). (**a**,**c**) The seasonal-mean precipitation and SST (1C° intervals; the 27 C° contour is highlighted in black). Side panels show the zonal mean precipitation. (**b**,**d**) The equatorially-symmetric components of the seasonal-mean precipitation, and the equatorially-symmetric component of SST seasonal-mean difference from the annual mean (solid/dashed black contours indicating positive/negative values at 0.5 °C intervals). Side panels show the zonal-means of the precipitation (blue) and seasonal SST anomaly (black). Precipitation and SST data taken from the Global Precipitation Climatology Project [GPCP; *Adler et al.*, 2003] dataset and from the Extended Reconstructed SST dataset (ERSST-v3b) provided by NOAA's National Climatic Data Center [*Smith et al.*, 2008], for 1998–2014.

here by introducing an idealized Bjerknes feedback, which captures the coupling of surface winds with tropical SSTs.

ITCZs are associated with the ascending branch of the tropical meridional overturning circulation; they are therefore an integral part of the tropical mean overturning circulation. Regions hosting a single ITCZ are characterized by monsoonal circulations, which are Hadley-like in the zonal mean [e.g., *Dima and Wallace*, 2003]. On the other hand, regions hosting double ITCZs that straddle the equator are associated with non–Hadley-like meridional overturning circulations: the double ITCZs lie along the rising branches of narrow meridional overturning circulations on either side of the equator, with a shared equatorial descending branch [*Bischoff and Schneider*, 2016; *Adam et al.*, 2016]. The bifurcation from single to double ITCZs is therefore linked to a bifurcation of the tropical overturning circulation [*Bischoff and Schneider*, 2016]. The position of ITCZs depends on factors such as surface moisture and momentum balances [e.g., *Lindzen and Nigam*, 1987; *Schneider and Bordoni*, 2008] and tropical wave dynamics [e.g., *Holton et al.*, 1971; *Gill*, 1980]; understanding the relation of these factors with the overturning circulation is therefore critical for a theory of tropical convergence zones. Additionally, in climate models, the transition from single- to double-ITCZ states is sensitive to the details of the convective scheme [e.g., *Möbis and Stevens*, 2012]. Nevertheless, even in such cases, the transition from single- to double-ITCZ states is closely associated with the mean circulation, reinforcing the need to explore the relation of ITCZs and the mean overturning circulation [*Voigt and Shaw*, 2015].

For simplicity, only the equatorially-symmetric component of the bifurcated ITCZ pattern is considered here. Specifically, this study focuses on: i) regional transitions from a single ITCZ to double ITCZs that straddle the equator, and ii) variations in the zonal orientation of ITCZs. These key modes of variation of the bifurcated ITCZ pattern are evident during the transition seasons, as shown in Fig. 1. During boreal spring (Fig. 1a), a double ITCZ that straddles the equator is observed in the eastern Pacific; a single ITCZ, which lies approximately along the equator, is observed outside the Pacific [e.g., *Zhang*, 2001]. (Note that during boreal spring, the southern branch of the double ITCZ in the eastern Pacific is distinct from the SPCZ, which extends diagonally from the equatorial western Pacific southeastwards to the subtropical central Pacific.) In contrast, during late boreal summer (Fig. 1c), a single ITCZ is observed in the eastern Pacific, and the Atlantic and Pacific ITCZs are farthest from the equator. Since regions of high precipitation tend to occur over regions of high SST [e.g., *Bjerknes*, 1969; *Trenberth and Shea*, 2005], these variations in the position of the ITCZs are strongly correlated with the variations in the positions of SST peaks (Fig. 1a,b).

Variations in the zonal orientation of the ITCZs become evident by examining the equatorially-symmetric component of the tropical precipitation, shown in Fig. 1b,d. During boreal spring, the ITCZs in the Pacific and Atlantic lie parallel to the equator; in contrast, during late boreal summer, the ITCZs are at their most diagonal orientation. This change in the zonal orientation of the ITCZs varies with the zonal SST gradients in the Pacific and Atlantic, which are minimal during boreal spring and maximal during late boreal summer [Fig. 1b,d; *Karnauskas et al.*, 2009], and with the mean tropical poleward SST gradient, which is strongest during boreal spring and weakest during late boreal summer (Fig. 1b,d). Similarly, the meridional extent of the Pacific and Atlantic cold tongues varies with the orientation of the ITCZs, from narrowest during boreal spring, to widest during late boreal summer. A similar variation in the orientation of the ITCZs is observed on inter-annual timescales; during strong El Niño episodes (i.e., like boreal spring, when eastern Pacific SSTs are elevated) the SPCZ becomes significantly more zonally oriented [*Vincent et al.*, 2011].

Here, the relation of the bifurcated ITCZ pattern to equatorially-symmetric zonal and meridional SST gradients is analyzed using a shallow water model on the equatorial beta plane, linearized about a state of rest, with prescribed heating and mechanical damping. Such models are known to capture the essential properties of equatorial wave dynamics, as shown by *Matsuno* [1966], and of thermally driven tropical circulations, as shown by *Gill* [1980], and are widely used in the study of large-scale tropical dynamics. Matsuno–Gill-type models can be interpreted as describing the first internal mode of the overturning circulation, with the meridional and zonal winds representing the vertical sheer between two atmospheric layers [*Matsuno*, 1966]. Given the idealized nature of these models, the prescribed heating and damping leave much room for interpretation. *Gill* [1980] described the diabatic heating as originating from latent heating associated with deep convection. This view, however, is problematic, as the ability of upper-troposphere diabatic heating to maintain lower-level convergence is uncertain [*Lindzen and Nigam*, 1987]. Instead, surface mass convergence linked to SST gradients has been shown to be critical for the maintenance of ITCZs [e.g., *Lindzen and Nigam*, 1987; *Waliser and Somerville*, 1994; *McGauley et al.*, 2004; *Sobel and Neelin*, 2006; *Raymond et al.*, 2006; *Back and Bretherton*, 2009]. Yet, despite the fundamental differences between the two views, with appropriate scaling of the idealized model, forcing the circulation by either prescribed diabatic heating or prescribed surface momentum fluxes is formally equivalent [*Neelin*, 1989]. Moreover, prescribing either diabtic heating or SST gradients neglects the strong coupling between the overturning circulation and SSTs. (See *Battisti et al.* [1999] for a discussion of the conceptual similarities and limitations of the two views.) Here it is shown that the bifurcated ITCZ pattern can form even with only idealized large-scale forcing, without prescribing localized diabatic heating or surface momentum fluxes.

Early observational analyses of the tropical free atmosphere [*Krishnamurti*, 1971a, b] revealed strong damping of the vorticity field [*Holton and Colton*, 1972]. Subsequent analyses using Matsuno–Gill-type models found damping rates of the order of 1–10 days [e.g., *Lin et al.*, 2008; *Romps*, 2014], in support of earlier findings. Here, in accordance with observations, solutions in the limit of strong damping are explored. It is shown that vorticity damping has a critical role in the emergence of the bifurcated ITCZ pattern. The model and motivation for seeking solutions in the viscous limit are presented in section 2. Approximate steady solutions are derived in section 3. Numerical steady solutions are presented in section 4, followed by a summary and discussion in section 5.

2. Model

2.1. Matsuno-Gill model in the viscous limit

The nondimensional Gill model [*Gill*, 1980] can be written as

$$-yv + \partial_x h = -\epsilon u \tag{1a}$$

$$yu + \partial_y h = -\epsilon v \tag{1b}$$

$$\partial_x u + \partial_y v = -Q \tag{1c}$$

where h is the deviation from mean geopotential height, u and v are the deviations of the zonal (along x) and meridional (along y) velocity components from a mean state of rest, and ϵ is the Rayleigh damping coefficient. As in *Matsuno* [1966], the equations are nondimensionalized using the phase speed of gravity waves $c \equiv \sqrt{gH}$, a time scale $T \equiv \sqrt{1/c\beta}$, and a length scale $L \equiv \sqrt{c/\beta}$ ($\beta = 2\Omega/a$ is the meridional derivative of the Coriolis parameter f at the equator, where Ω and a are Earth's rate of rotation and radius). The effective height (H) of the model is therefore linked to the time and length scales, as well as the source term Q [*Gill*, 1982]. Similarly, the effective timescale of the Rayleigh damping is not directly related to observed values, but depends on the scaling parameters. An important distinction between Eq. (1) and the Gill model is that the damping term ϵv is not neglected in Eq. (1b). For the large-scale circulation in the limit of small ϵ, this term becomes negligible [*Gill*, 1980]. However, since solutions in the limit of large ϵ are explored here, this common simplification of the model is not applied in Eq. (1).

From the steady continuity equation, the vertical velocity is given by

$$w = -\partial_x u - \partial_y v = Q. \tag{2}$$

Accordingly, the signs of u and v correspond to near-surface winds; h is proportional to positive surface pressure anomalies and, near the equator, to negative SST anomalies. Since deep convection is strongly coupled to vertical winds, positive peaks of the vertical wind are referred to here as ITCZs.

2.2. The viscous limit

It is helpful to write Eq. (1) in terms of the divergence $\delta \equiv \partial_x u + \partial_y v$ and relative vorticity $\xi \equiv \partial_x v - \partial_y u$. Taking the curl of the momentum equations yields

$$y\delta = -v - \epsilon\xi. \tag{3a}$$

The divergence of the momentum equations yields

$$\epsilon\delta = y\xi - u - (\partial_{xx} + \partial_{yy})h \tag{3b}$$

and the continuity equation becomes

$$\delta = -Q. \tag{3c}$$

By combining Eqs. (3a) and (3c), we find

$$yQ = v + \epsilon\xi. \tag{4}$$

Gill [1980] noted that in the inviscid limit ($\epsilon \to 0$), Eq. (4) becomes analogous to the Sverdrup balance in oceanography, $yQ = v$, so that near-surface flow is poleward in the heating region and equatorward in the cooling region – a well observed feature of the first internal mode of the tropical circulation, as shown in Fig. 2 for the Pacific sector [cf. *Adames and Wallace*, 2014]. In the viscous limit, vorticity damping cannot be neglected and the resulting balance (Eq. 4) is analogous to the Stommel model [*Stommel*, 1948] (see next section).

The association of Q with both large-scale processes and diabatic heating directly related to deep convection poses a scaling problem. Since deep convection occurs on relatively short time scales ($\sim$ hours) and small length scales ($\sim$ a few kilometers), a scale separation exists between the balanced large-scale tropical circulation (with time scales of days or longer and length scales of thousands of kilometers) and the transient circulation directly related to deep convection [*Ooyama*, 1982; *Raymond et al.*, 2015]. Formally, where convection occurs, Eq. (3c) becomes

$$\delta' \approx -Q'_c \tag{5}$$

where $(\ )'$ denotes perturbations on spatial and temporal scales relevant to processes associated with deep convection, and Q'_c denotes diabatic heating associated with deep convection. The vorticity equation (3b) then becomes

$$yQ'_c = v' + \epsilon'\xi'. \tag{6}$$

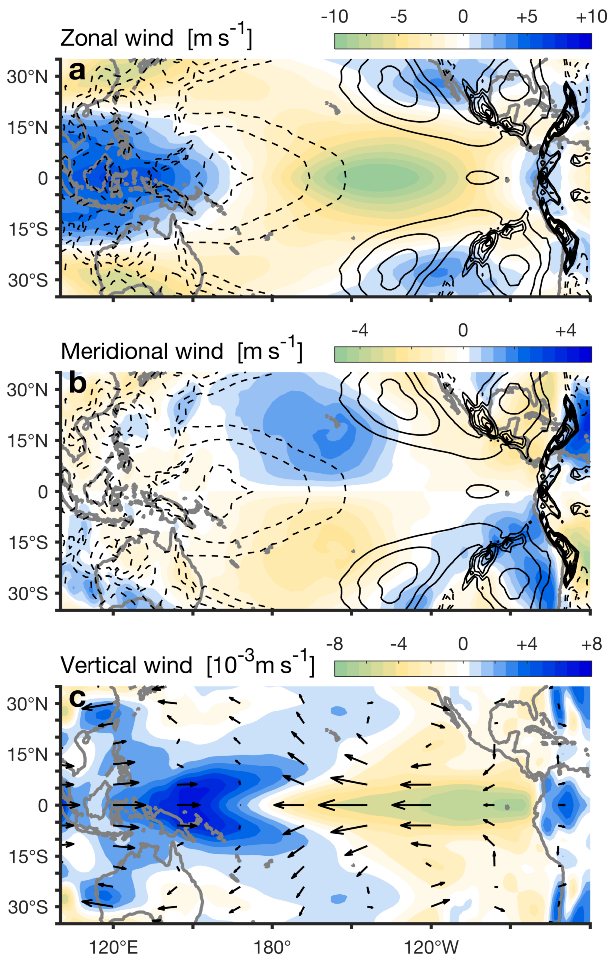

Figure 2. Equatorially-symmetric annual-mean zonal anomaly of the sea-level pressure and wind in the Pacific sector. (**a**,**b**) Sea-level pressure (solid/dashed black contours indicate positive/negative anomalies at 0.5 hPa intervals) and the difference between the 700–1000 and 200–500 hPa levels of the zonal (**a**) and meridional (**b**) winds. (**c**) The vertical wind at the 500 hPa level and the net (zonal and meridional from panels **a** and **b**) horizontal wind (arrows). Data taken from the European Center for Medium-Range Weather Forecasts (ECMWF) Interim Reanalysis [*Dee et al.*, 2011] for 1979–2014.

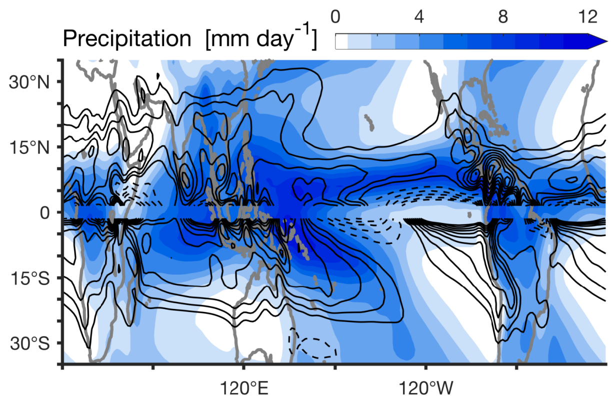

Figure 3. Annual-mean precipitation (blue) and the difference between the 700–1000 and 200–500 hPa levels annual-mean local Rossby number, $-\xi/f$, calculated in spherical coordinates (solid/dashed black contours indicate negative/positive values at 0.1 intervals; equatorial values are not shown). Data taken from the European Center for Medium-Range Weather Forecasts (ECMWF) Interim Reanalysis [*Dee et al.*, 2011] for 1979–2014.

In the observed atmosphere, the intense diabatic heating associated with deep convection is predominantly balanced by nonlinear and dissipative terms which are represented in the linear model by vorticity damping [e.g., *Sardeshmukh and Held*, 1984]. Therefore, from Eq. (6), the diabatic heating associated with deep convection is approximately given by

$$Q_c' \approx \frac{\epsilon'}{y}\xi'. \tag{7}$$

Equation (7) implies that ITCZs, which are dominated by deep convection, lie along minimal values of the first internal mode of the local Rossby number $-\xi/y$. This relation is indeed roughly consistent with observations, as shown in Fig. 3. Substituting for δ and ξ in Eq. (3b) using Eqs. (5) and (7) yields in the limit of large ϵ'

$$Q_c' \approx \frac{\epsilon'^2 + y^2}{\epsilon'}(\partial_{xx} + \partial_{yy})h' \tag{8}$$

which implies that the ITCZ position follows SST peaks – a well known observed property of ITCZs [Fig. 1; *Trenberth and Shea*, 2005]. Thus, a direct implication of Eqs. (7) and (8), supported by Figs. 1 and 3, is that the idealized model is most suited for studying the large-scale features of ITCZs in the viscous limit.

2.3. Forcing

The source term Q consists of relaxation to a prescribed zonally asymmetric surface pressure (Q_W), convective heating coupled to the vertical wind (Q_c), and sensible cooling associated with equatorial upwelling (Q_E)

$$Q = Q_W + Q_c + Q_E. \tag{9}$$

The term Q_W mimics relaxation to an equilibrium zonal pressure gradient, which drives a zonal-overturning, Walker-like circulation

$$Q_W(x,y) = \epsilon\big(h - \bar{h}\big) \tag{10}$$

with the relaxation height

$$\bar{h}(x,y) = A\sin(2\pi x/L)e^{-y^2/2\sigma^2} \tag{11}$$

where L is the length of the periodic zonal domain, and negative values of the constant A correspond to high surface pressure in the eastern part of the domain, and low pressure to the west. Q_W is formally identical to the source used by *Matsuno* [1966] for $\sigma = 1$. Since A and σ set the equilibrium zonal and poleward surface pressure gradients, the sensitivity of the steady states of the model to variations in these parameters is explored here. The parameter ϵ is inversely proportional to both the mechanical damping time in the momentum equations, and the overturning relaxation time in the continuity equation. In the viscous limit, this corresponds to unrealistically short overturning circulation times. Nevertheless, as in the inviscid case [*Gill*, 1980], the solutions are found to be qualitatively insensitive to this duality of ϵ.

For the convective source term Q_c, it is assumed that upward large-scale motion increases convective heating, and downward motion increases diabatic cooling [e.g., *Gill*, 1982]

$$Q_c = -\gamma\delta. \tag{12}$$

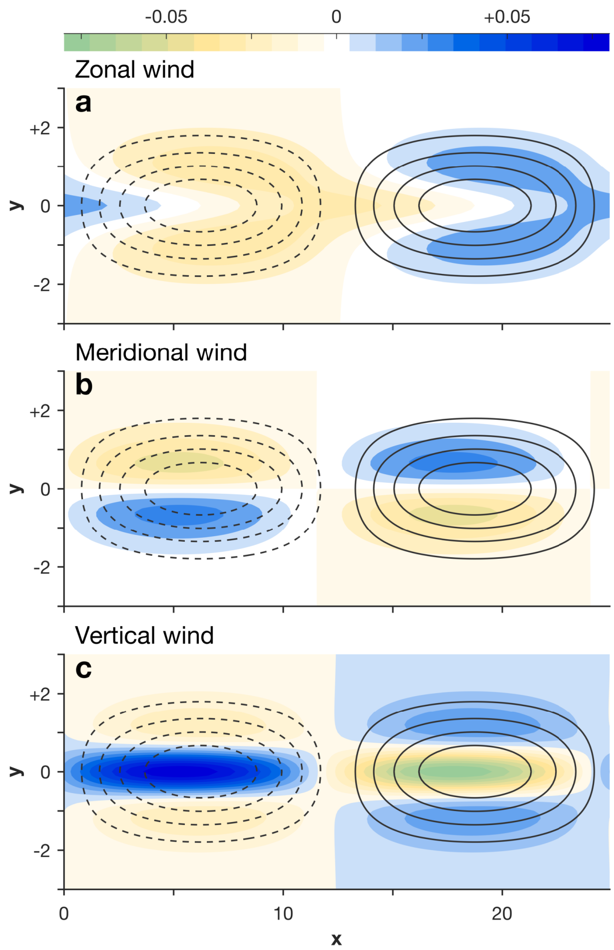

Figure 4. Relaxation height $\bar{h}$ (solid/dashed black contours indicate positive/negative values at 0.02 intervals) and the solution in the viscous limit for the zonal wind (**a**, Eq. 17a), meridional wind (**b**, Eq. 17b) and vertical wind (**c**, Eq. 18). The model parameters are: $A = -0.1, \sigma = 1, \epsilon = 1, \gamma = 0$, and $C_E = 0$.

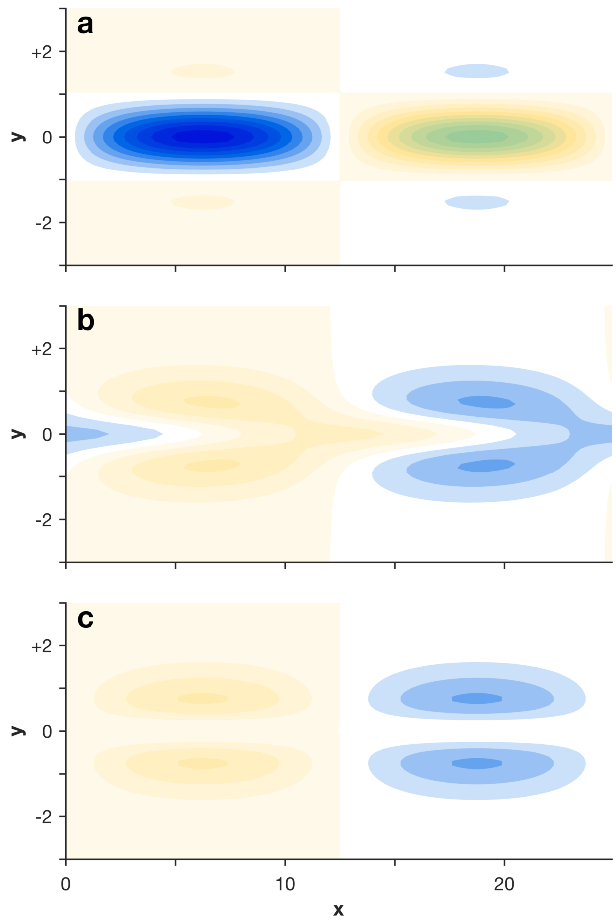

Figure 5. The contributions of terms a, b, and c (with matching panel letters) in Eq. (18) to the vertical wind shown in Fig. 4c (with matching contours).

For $1 < \gamma$, the divergence term in the continuity equation becomes convergent, leading to unstable solutions of the time-dependent equations. Therefore, the convective coupling constant is constrained to $0 \leq \gamma < 1$. It is important to note that this common parameterization is consistent with the notion that convective heating does not independently drive the large-scale circulation, but rather acts to enhance the relaxation towards equilibrium [*Emanuel et al.*, 1994]. This is readily seen in the following example: for $Q = \epsilon(h - \bar{h}) - \gamma\delta$, in the limit of $\gamma \to 1$, Eq.(3c) yields $h = \bar{h}$; in other words, h approaches the prescribed equilibrium height as the convective coupling strengthens.

Finally, surface winds and SSTs are coupled via oceanic Ekman balance [e.g., *Schneider et al.*, 2014; *Green and Marshall*, 2017]. Specifically near-surface ocean currents (u_o, v_o) are assumed to be balanced by surface wind stress (τ_x, τ_y)

$$y u_o = \tau_y \tag{13a}$$

$$y v_o = -\tau_x. \tag{13b}$$

This balance drives oceanic upwelling where the surface currents diverge, which leads to surface cooling. Thus, assuming that the stress is linearly related to the surface wind, the heating associated with the Ekman coupling is given by

$$Q_E = -C_E \left[\partial_x \left(\frac{v}{y} \right) - \partial_y \left(\frac{u}{y} \right) \right] \tag{14}$$

where the Ekman coupling coefficient C_E relates the upwelling and its associated surface cooling to an increase in surface pressure. To account for the equatorial latitude belt where the Ekman balance does not hold (i.e., where $y \to 0$), and to account for the fact that surface warming in regions of ocean downwelling is generally negligible compared to the cooling in upwelling regions, the Ekman coupling is represented as

$$F_{Ek} = \partial_x \left(\frac{yv}{y_0^2 + y^2} \right) - \partial_y \left(\frac{yu}{y_0^2 + y^2} \right) \tag{15a}$$

and the associated heating is given by

$$Q_E = -C_E \mathcal{H}(F_{Ek}) F_{Ek} \tag{15b}$$

where the parameter y_0 can be interpreted as the oceanic Rossby radius of deformation near the equator (~200km, [*Gill*, 1982]) or as representing dissipative effects in the oceanic mixed layer [*Codron*, 2012], and $\mathcal{H}$ is a heavyside step function. The results were found to be qualitatively insensitive to the value of y_0, which is set to 0.2 in all of the numerical solutions (Sec. 4).

The source terms $Q_W + Q_E$ comprise an idealized Bjerknes feedback [*Bjerknes*, 1969; *Neelin*, 2011], driving an ide-

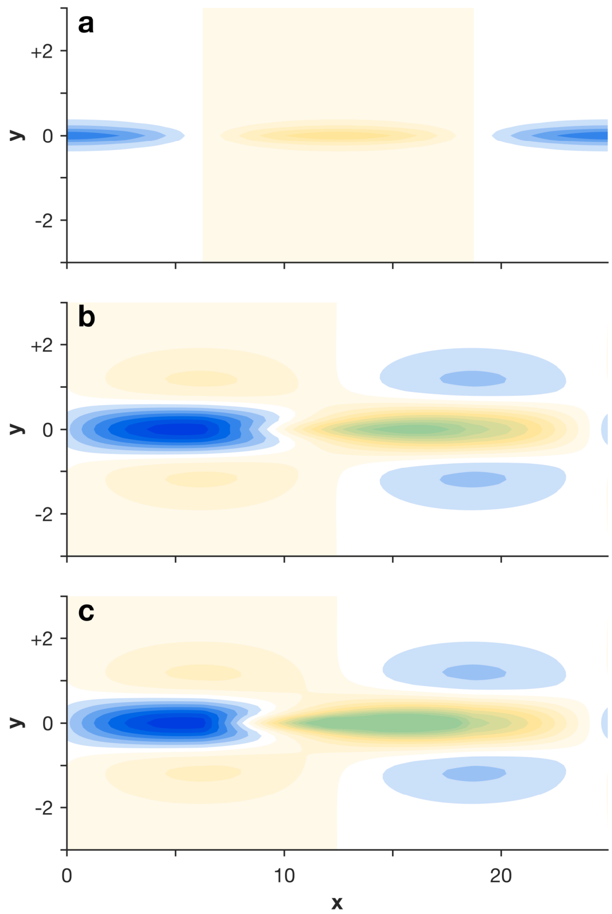

Figure 6. Approximate solutions of the vertical wind in the viscous limit of the Bjerkness feedback. (**a**) The approximation of the near-equator vertical wind (color, Eq. 20) for $C_E = 0.1$. (**a**,**b**) The superposition of approximations (18) and (20) for $C_E = 0.1$ (**a**) and $C_E = 0.2$ (**b**). The other model parameters are: $\epsilon = 1, A = -0.1, \gamma = 0$, and $\sigma = 1$. Contour surfaces are constrained between ± 0.14 with 21 intermediate values.

alized Walker circulation which is coupled to the underlying oceanic circulation. In the following sections, the contributions of each of the above source terms to the large-scale circulation associated with ITCZs are examined in the viscous limit.

3. Approximate solutions

3.1. The viscous Walker circulation

The steady circulation with no Ekman coupling ($C_E = 0$) in the limit of large ϵ is first considered. To leading order in ϵ, the continuity equation (1c) yields

$$h \approx \bar{h} \tag{16}$$

(as shown above, this approximation becomes an identity in the limit $\gamma \to 1$). Under this approximation, Eq. (1c) decouples from Eqs. (1a,b) and the momentum Eqs. (1a,b) can be solved independently by substituting h from Eq. (4)

$$u = -\frac{\epsilon}{\epsilon^2 + y^2}\partial_x \bar{h} - \frac{y}{\epsilon^2 + y^2}\partial_y \bar{h} \tag{17a}$$

$$v = \frac{y}{\epsilon^2 + y^2}\partial_x \bar{h} - \frac{\epsilon}{\epsilon^2 + y^2}\partial_y \bar{h}. \tag{17b}$$

(Note that in the zonal mean, these expressions for the surface wind differ from those obtained by *Schneider and Bordoni* [2008] who used a nonlinear idealized model; however, the dependence on the meridional gradient of $\bar{h}$ is similar in both expressions.) As shown in Fig. 4, in the viscous limit, the resulting meridional wind is opposite to the Sverdrup balance; it is poleward in the cooling region and equatorward in the heating region.

From Eq. (3c), in the viscous limit, the vertical wind in the zonal overturning circulation forced by Q_W is given by

$$w_W = \overbrace{\frac{\epsilon}{\epsilon^2 + y^2}(\partial_{xx} + \partial_{yy})\bar{h}}^{a} + \overbrace{\frac{y^2 - \epsilon^2}{(\epsilon^2 + y^2)^2}\partial_x \bar{h}}^{b} \overbrace{- \frac{2\epsilon y}{(\epsilon^2 + y^2)^2}\partial_y \bar{h}}^{c}. \tag{18}$$

As shown in Fig. 4c, Eq. (18) implies that in the viscous limit, upward winds are induced near surface pressure lows (term a), negative (positive) zonal pressure gradients (term b) for $y < \epsilon$ ($y > \epsilon$), and negative poleward pressure gradients (term c). As shown in Fig. 5a, term a (Fig. 5a) generates a rising branch in the low-pressure (Low) node of the forcing and a descending branch in the high-pressure (High) node of the forcing. The zonal and meridional gradient terms (terms b and c shown in Fig. 5b,c) damp the single ITCZ that forms in the Low node and induce a double ITCZ that straddles the equator in the High node. Thus, a bifurcated ITCZ pattern emerges in the viscous limit for zonally asymmetric large-scale forcing.

3.2. The Bjerkness feedback in the viscous limit

Substituting for u/y from Eq. (1a) and for v/y from Eq. (1b) in Eq. (14) gives

$$Q_E = -\frac{C_E}{\epsilon}\left(\partial_x u + \partial_y v + \frac{\partial_x h}{y^2}\right). \tag{19}$$

Therefore, the Ekman source term dominates and intensifies the vertical wind near the equator. Combined with the convective source term, this gives

$$w_E \approx -\frac{C_E}{\epsilon(1-\gamma) - C_E}\frac{\partial_x \bar{h}}{y_0^2 + y^2} \tag{20}$$

near the equator, where Eq. (18) is used to approximate h and y_0 is utilized as in Eq. (15b). Figure 6a shows w_E for $C_E = 0.1$ and $\epsilon = 1$. Indeed, as expected, a narrow high-pressure band with intense descending winds emerges along the equator in regions where the zonal surface pressure gradient is positive, mimicking the Pacific and Atlantic cold tongues. As in the convective coupling case, this approximation predicts unstable solutions for

$$\gamma^* \equiv \gamma + C_E/\epsilon > 1, \tag{21}$$

ensuring $w_E \propto -\partial_x \bar{h}$ for all stable steady solutions. In practice, unstable numerical integrations of the time-dependent equations (see next section) were found to occur for γ^* values as low as 0.2.

The full effect of the idealized Bjerkness feedback is captured by the superposition of the approximate solutions of the vertical wind (Eqs. 18 and 20) $w_B \equiv w_W + \mathcal{H}(-w_E)w_E$, which is shown for $C_E = 0.1$ in Fig. 6b and for $C_E = 0.2$ in Fig. 6c. The cold tongue extends into the rising branch of the zonal overturning circulation with increasing C_E. In addition, as the cold tongue extends into the Low region, it creates a diagonal cleavage in the rising branch of the zonal overturning circulation (Fig. 6b,c), mimicking the observed splitting of the vertical wind in the western Pacific (Fig. 2c). This splitting of the ITCZ in the Low node is consistent

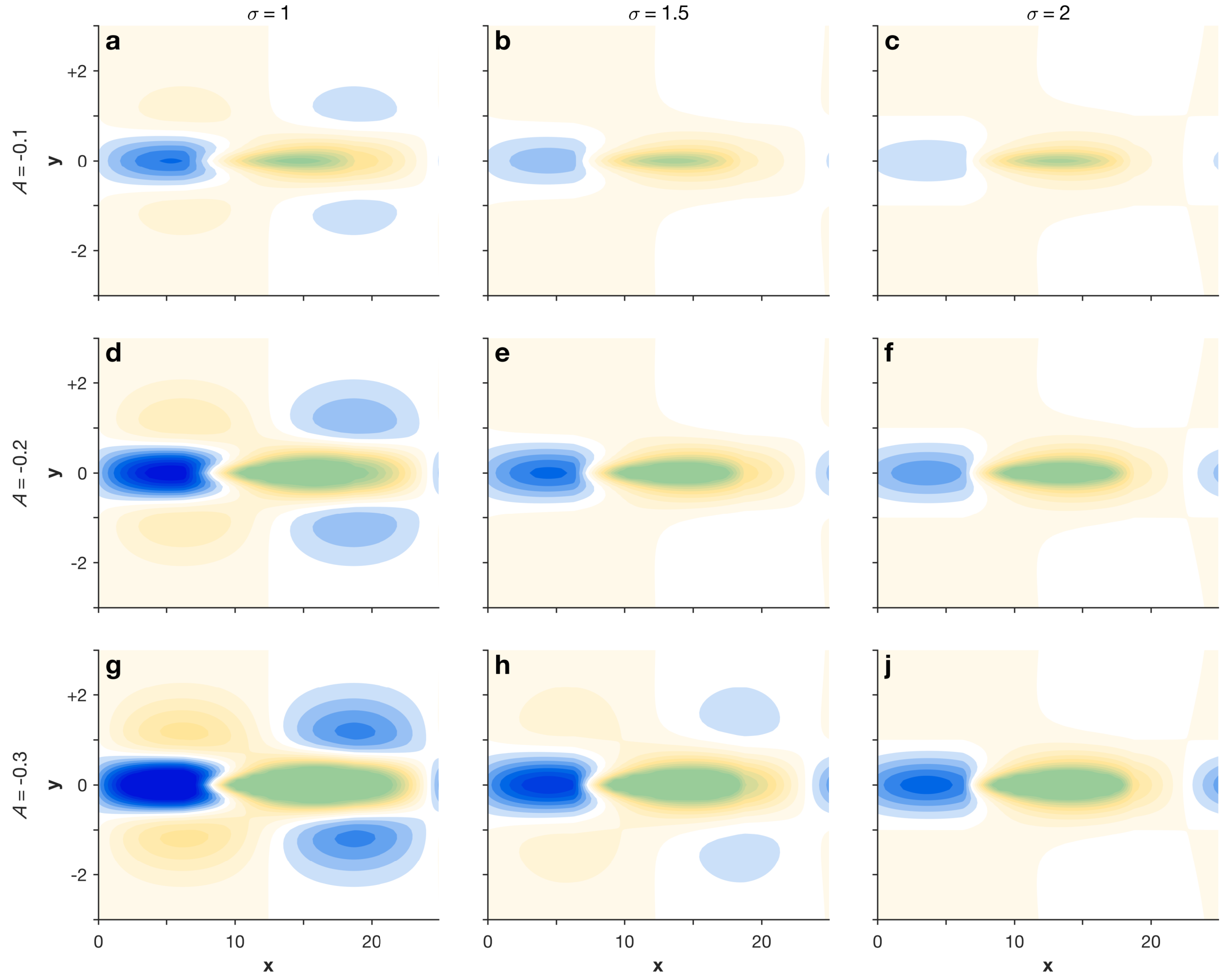

Figure 7. The dependence of the vertical wind on zonal and poleward gradients of the relaxation height in the approximate solutions in the viscous limit (the superposition of approximations 18 and 20). Zonal gradients increase with the constant A (Eq. 11) down columns; poleward gradients weaken with increasing σ (Eq. 11) along rows. The other model parameters are: $\epsilon = 1, \gamma = 0$, and $C_E = 0.2$. Contour surfaces are constrained between ± 0.21 with 21 intermediate values.

with the mechanism proposed by *Bischoff and Schneider* [2016] whereby for sufficiently strong oceanic heat uptake, the mean meridional circulation bifurcates from a single ITCZ circulation with equatorial ascent to a double-ITCZ circulation with an equatorial descending branch. In the High node, this mechanism reinforces, but does not drive, the double ITCZ which emerges in the viscous limit (Fig. 4).

To study the dependence of the bifurcated ITCZ pattern on zonal and poleward pressure gradients, the dependence of w_B on variations in the parameters A and σ is analyzed in Fig. 7. Consistent with observations (Fig. 1), the cold tongue widens with increasing zonal pressure gradients (i.e., as A becomes more negative) and with weakening poleward gradients (i.e., with increasing σ). Similarly, the double ITCZ in the High node weakens relative to the single ITCZ in the Low now with weakening poleward gradients. Next, the approximate solutions are compared with exact numerical steady solutions of the model.

4. Numerical solutions

Steady states are obtained by time integrations of the model (i.e., time derivatives are added on the left-hand side of Eq. 1) from a resting state using a leap-frog scheme for 100 days. Explicit numerical diffusion other than Rayleigh damping is not used. The results are qualitatively insensitive to the details of the integration scheme.

Figure 8 shows steady-state solutions of the model forced by relaxation to a zonally asymmetric equilibrium height. For small ϵ, the solutions are similar to those shown by *Matsuno* [1966] (compare Fig. 8a,d with Fig. 9 in *Matsuno* [1966]). In the viscous limit, the numerical solutions are well captured by the analytic solutions (4) and (18) (compare Fig. 8e,f with Fig. 4b). As predicted by the theory, in the viscous limit $h \approx \bar{h}$ (Fig. 8b) and a double ITCZ appears in the High node (Fig. 8e). The addition of convective coupling causes the double ITCZs to intensify and shift closer to the equator, but by itself does not lead to the emergence of the bifurcated pattern (Fig. 8f).

The effect of Ekman coupling is shown in Fig. 9, where the circulation is forced by the same zonally asymmetric relaxation height as in Fig. 8 but with $C_E > 0$. For small ϵ, the solutions substantially differ from those found by *Matsuno* [1966] (compare Figs. 8a,d and 9a,d); the emergent Walker circulation has a narrow rising branch and a dominant cold tongue in the descending branch. As in the approximate solutions (Fig. 6), the cold tongue produced by the Ekman coupling opens a chasm in the rising branch of the zonal overturning circulation. The split ITCZs in the rising branch of the zonal overturning circulation nearly merge with the double ITCZs in the descending branch of the zonal overturning circulation as ϵ and C_E are increased (Fig. 9f).

As in Fig. 7 for the approximate solutions, the dependence of the steady vertical wind in the numerical solutions

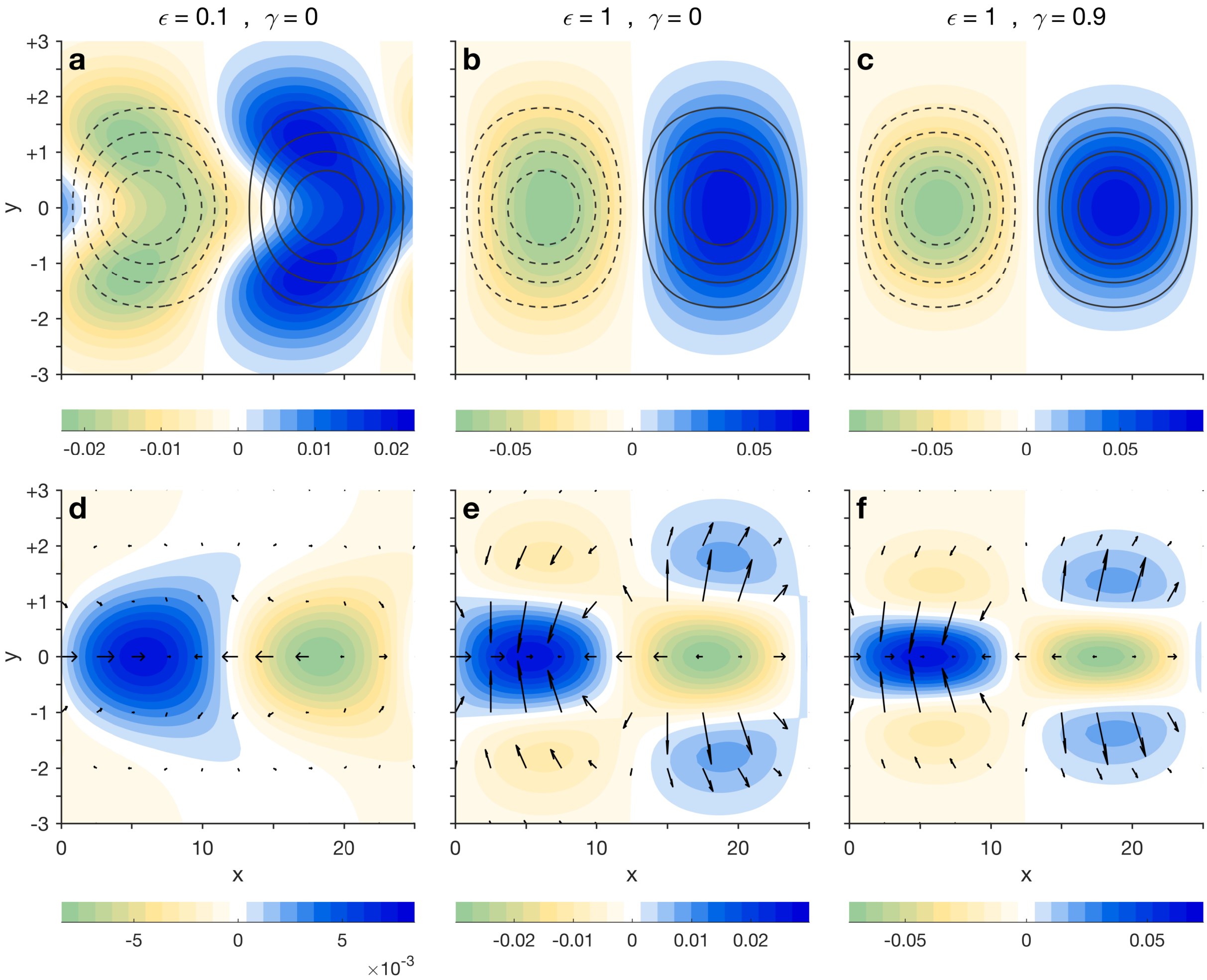

Figure 8. The relaxation height $\bar{h}$ (contours, 0.02 intervals, upper panels) and numerical steady solutions of the height (color, upper panels), vertical wind (color, lower panels) and surface winds (arrows, lower panels) for the model forced by $Q = Q_W + Q_c$. Results are shown for $\epsilon = 0.1$ (left column), $\epsilon = 1$ (middle column), and $\epsilon = 1$ with strong convective coupling ($\gamma = 0.9$, right column). The other model parameters are: $A = -0.1, C_E = 0$, and $\sigma = 1$.

on variations in the parameters A and σ is analyzed in Fig. 10. The numerical solutions are well captured by the theory (Fig. 7), with the exception that the cold tongue and the variations in the orientation of the ITCZs are more pronounced in the numerical solutions. Consistent with observations, the cold tongue strengthens with increasing zonal gradients and its base widens with weakening poleward gradients, thereby controlling the emergence and orientation of the double ITCZs in the High node.

5. Summary and discussion

A simple shallow water model on the equatorial beta plane with an idealized Bjerknes feedback is employed to study the equatorially symmetric features of the bifurcated ITCZ pattern. It is shown that analysis of the large-scale features of ITCZs using the idealized model is consistent with observations in the limit of strong damping.

Two ITCZ bifurcation mechanisms are identified:

1. In the viscous limit, upward winds go along with negative anomalies of the local Rossby number (Eq. 4, Fig. 2), which form along the equator for surface Lows and off the equator for surface Highs. This leads to a bifurcated ITCZ pattern with a single ITCZ in the heating region, and a double ITCZ that straddles the equator in the cooling region (Fig. 4). The emergent pattern mimics the observed regional bifurcation from a single ITCZ over the Indian Ocean to ITCZs on either side of the equator in the Pacific (Figs. 1,2,3), and captures the emergence of a double ITCZ that straddle the equator in the eastern Pacific during boreal spring (Fig. 1) for sufficiently strong poleward temperature gradients (Figs. 7,10).

2. Surface wind stress induces equatorial ocean upwelling which cools the surface. The cooling increases surface pressure, which, in turn, reduces vertical winds near the equator. The idealized Bjerknes feedback captures this effect, leading to an equatorial cold tongue (Fig. 6), mimicking the observed equatorial cold tongue in the Atlantic and Pacific (Figs. 1,2). As the cold tongue intensifies and extends into the rising branch of the Walker circulation, it opens a diagonal cleavage in the rising branch of the zonal overturning circulation which resembles a split ITCZ (Fig. 6). This mechanism mimics the observed splitting of the ITCZ in the western Pacific (Fig. 2) and may reinforce the observed bifurcation to a double ITCZ that straddle the equator in the eastern Pacific during boreal spring [*Adam et al.*, 2016].

Thus, the bifurcated ITCZ pattern emerges in the viscous limit. Analytic approximate solutions in the viscous limit capture the emergence of the bifurcated ITCZ pattern, as well as the dependence of the bifurcated ITCZ pattern on

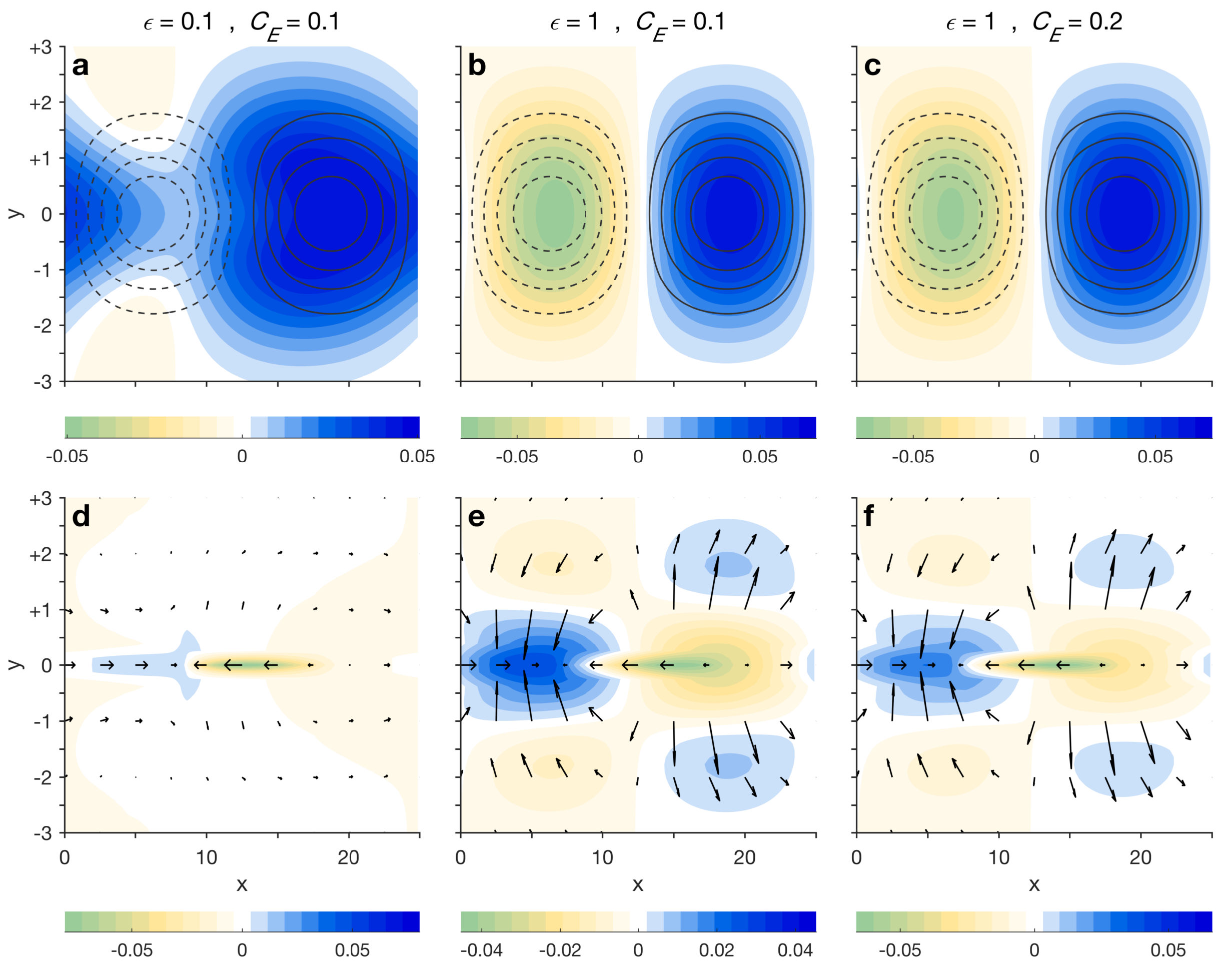

Figure 9. The relaxation height $\bar{h}$ (contours, 0.02 intervals, upper panels) and numerical steady solutions of the height (color, upper panels), vertical wind (color, lower panels) and surface winds (arrows, lower panels) for the model forced by $Q = Q_W + Q_c + Q_E$. The values of ϵ and C_E are shown at the top of each column. The other model parameters are: $A = -0.1, \gamma = 0$, and $\sigma = 1$.

zonal and poleward SST gradients. Consistent with observations, the cold tongue intensifies with increasing zonal SST gradients, and its base widens with weakened poleward SST gradients, modulating the zonal orientation of the ITCZs on either side of the cold tongue (Figs. 1,7,10).

The solutions of the idealized model in the viscous limit provide insight on the origin of the large-scale bifurcated ITCZ pattern, but at the cost of filtering out key processes which determine the exact position and structure of ITCZs. These include boundary layer dynamics [e.g., *Sobel and Neelin*, 2006; *Back and Bretherton*, 2009; *Schneider and Bordoni*, 2008; *Gonzalez et al.*, 2016] and the role of wave dynamics in setting the preferred locations of convergence zones [e.g., *Holton et al.*, 1971; *Gill*, 1980]. Additionally, due to the absence of meridional advection, the ITCZs in the idealized model are much broader than observed [e.g., *Gonzalez et al.*, 2016].

A major caveat of the theory is that, in contrast to observations which are consistent with the Sverdrup balance (Fig. 3), in the limit of strong vorticity damping the Sverdrup balance is reversed (Fig. 4). This discrepancy is potentially related to the idealized Rayleigh damping, which represents a mix of processes with potentially different spatial and temporal scales (Sec. 2.2). It acts as an overturning relaxation time in the source terms, which becomes unrealistically short in the viscous limit. In the momentum equations, the damping can be interpreted as representing either surface momentum fluxes in the surface branch of the overturning circulation, or cumulus drag and nonlinear terms in the upper branch of the overturning circulation. Moreover, some speculation remains regarding the origin of the observed strong damping in the free atmosphere, making it difficult to associate the vertical winds induced in the limit of strong damping with specific processes. In particular, the degree to which the linear momentum drag represents cumulus friction or nonlinear terms is not clear [*Sardeshmukh and Held*, 1984]. Additionally, observed cumulus momentum transport is spatially inhomogeneous and related to the convection intensity and vertical structure [*Lin et al.*, 2008; *Romps*, 2014] – features which are not represented by the Rayleigh damping.

Nevertheless, the essential features of the observed bifurcated ITCZ pattern are captured in the idealized model. Specifically, concurrent single and double ITCZs emerge in the steady solutions without explicitly prescribing local SST gradients or diabatic heating (Fig. 4). Therefore, the idealized model suggests the following mechanism for the emergence of the bifurcated ITCZ pattern: The existence of a Bjerknes feedback mandates a zonally asymmetric surface pressure distribution over ocean basins; given sufficiently strong surface turbulent fluxes, surface convergence zones will form along the equator in the Low node of the surface pressure and on either side of the equator in the High node; vertical motion in these convergence zones will in turn be amplified by the coupling of the atmospheric circulation with convective heating; the coupling of the atmospheric and

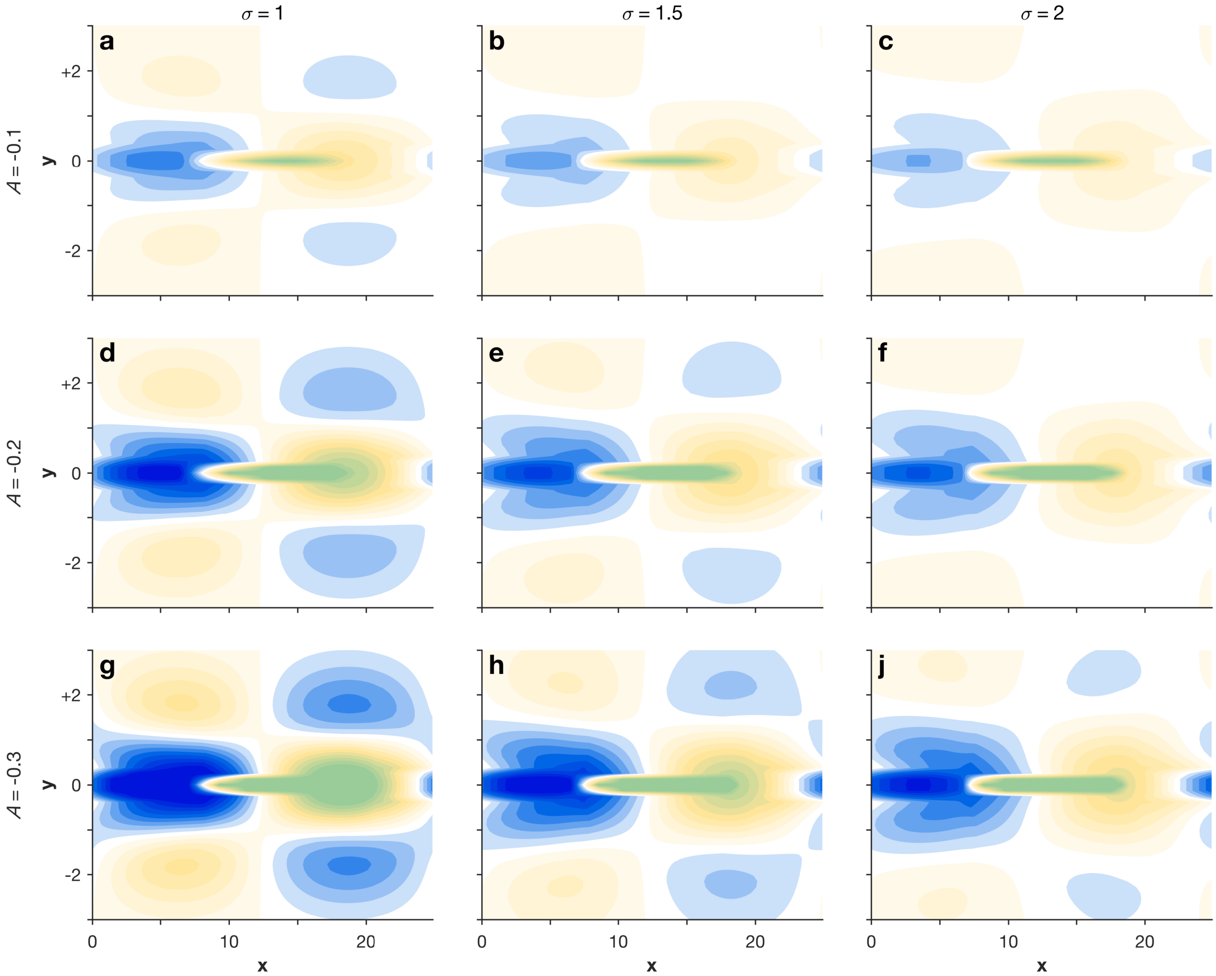

Figure 10. As in Fig. 7 for the numerical solutions. Contour surfaces are constrained between ±0.67 with 21 intermediate values.

oceanic circulations via Ekman balance generates an equatorial cold tongue which extends into and splits the single ITCZ in the Low node, and modulates the orientation and position of the double ITCZs that straddle the equator in the High node.

In both inviscid and viscous theory, the zonal extent of the rising branch of the Walker circulation is smaller than the extent of the descending branch, but for different reasons. *Gill* [1980] associated the relative narrowness of the rising branch with the difference in the phase speeds of westward propagating equatorial Rossby waves and eastward propagating Kelvin waves, which arise from localized heating. In contrast, in the viscous limit, equatorial waves are completely damped. Instead, the intrusion of the cold tongue into the rising branch of the zonal overturning circulation reduces winds there, thereby extending the descending branch at the expense of the rising branch.

Dynamical studies of the south Pacific convergence zone (SPCZ) have shown that it owes its diagonal orientation to the existence of a Pacific cold tongue which creates diagonal SST peaks on either side of the equator [e.g., *van der Wiel et al.*, 2016], but that the convection intensity in the SPCZ is strongly influenced by diagonal wave trains which dissipate over regions with elevated SSTs [e.g., *Widlansky et al.*, 2011; *van der Wiel et al.*, 2015]. Unlike observations, the ITCZs in the idealized model nearly vanish where the single and double ITCZs merge (Figs. 8f and 7f). This may reflect the absence of convective dissipation of subtropical storms in the idealized model. Similarly, the origin of the nearly-equinoctial variation in the orientation of ITCZs (Fig. 1), which is inextricably linked to the atmospheric and oceanic overturning circulations, is not well understood and may likewise be linked to subtropical eddy activity.

The idealized Bjerknes feedback provides a conceptual framework for studying the large-scale features of ITCZs and the tropical circulation. In particular, it can be used to study the nature of tropical precipitation biases in climate models, which are known to be strongly correlated with cold tongue biases [e.g., *Lin*, 2007; *Adam et al.*, 2017] and with the tendency of climate models to overestimate precipitation in ascent regions [*Oueslati and Bellon*, 2015]. Similarly, the effect of trends in SST gradients, such as those observed in the equatorial Pacific [*Karnauskas et al.*, 2009], can be examined using fundamental parameters. Most importantly, it links tropical precipitation variations with irreversible processes in the atmosphere in a manner hitherto unexplored.

Acknowledgments. I thank Nathan Paldor, Tapio Schneider, Rodrigo Cabellero and Yair Cohen for their insights. This research is supported by the Israeli Science Foundation grant 1185/17. Simulation results and model source code are available at *www.oriadam.info/goat/GillModel.zip*. O. Adam thanks the NASA/Goddard Space Flight Center's Laboratory for Atmospheres for providing the GPCP combined precipitation data, NOAA's National Centers for Environmental Information for providing the ERSST data, and the European Center for Medium-Range Weather Forecasts (ECMWF) for providing the ERA-Interim reanalysis data.

References

Adam, O., T. Bischoff, and T. Schneider (2016), Seasonal and interannual variations of the energy flux equator and ITCZ. Part II: Zonally varying shifts of the ITCZ, *J. Climate*, *29*, 7281–7293, doi:10.1175/JCLI-D-15-0710.1.

Adam, O., T. Schneider, and F. Brient (2017), Regional and seasonal variations of the double-ITCZ bias in CMIP5 models, *Climate Dynamics*, *43*, doi:10.1007/s00382-017-3909-1.

Adames, A. F., and J. M. Wallace (2014), Three-dimensional structure and evolution of the mjo and its relation to the mean flow, *Journal of the Atmospheric Sciences*, *71*(6), 2007–2026, doi:10.1175/JAS-D-13-0254.1.

Adler, R. F., G. J. Huffman, A. Chang, R. Ferraro, P.-P. Xie, J. Janowiak, B. Rudolf, U. Schneider, S. Curtis, D. Bolvin, A. Gruber, J. Susskind, P. Arkin, and E. Nelkin (2003), The Version-2 Global Precipitation Climatology Project (GPCP) monthly precipitation analysis (1979-present), *J. Hydrometeor.*, *4*, 1147–1167.

Back, L. E., and C. S. Bretherton (2009), On the relationship between SST gradients, boundary layer winds, and convergence over the tropical oceans, *Journal of Climate*, *22*(15), 4182–4196, doi:10.1175/2009JCLI2392.1.

Battisti, D. S., E. S. Sarachik, and A. C. Hirst (1999), A consistent model for the large-scale steady surface atmospheric circulation in the Tropics, *J. Atmos. Sci.*, *12*, 2956–2964.

Bischoff, T., and T. Schneider (2016), The equatorial energy balance, ITCZ position, and double ITCZ bifurcations, *J. Climate*, *29*, 2997–3013, doi:10.1175/JCLI-D-15-0328.1.

Bjerknes, J. (1969), Atmospheric teleconnections from the equatorial Pacific, *Mon. Wea. Rev.*, *97*, 163–172.

Bony, S., G. Bellon, D. Klocke, S. Sherwood, S. Fermepin, and S. Denvil (2013), Robust direct effect of carbon dioxide on tropical circulation and regional precipitation, *Nature Geosci.*, *6*, 447–451.

Boos, W. R., and R. L. Korty (2016), Regional energy budget control of the intertropical convergence zone and application to mid-Holocene rainfall, *Nature Geoscience*, *9*, 892–897, doi: 10.1038/ngeo2833.

Codron, F. (2012), Ekman heat transport for slab oceans, *Clim. Dyn.*, *38*, 379–389.

Dee, D., S. M. Uppala, A. J. Simmons, P. Berrisford, P. Poli, S. Kobayashi, U. Andrae, M. Balmaseda, G. Balsamo, P. Bauer, P. B. A.C.M., Beljaars, L. van de Berg, J. B. N., Bormann, C. Delsol, R. Dragani, M. Fuentes, A. Geer, L. Haimberger, S. Healy, H. Hersbach, E. Holm, L. Isaksen, P. Kallberg, M. Kohler, M. Matricardi, A. McNally, B. Monge-Sanz, J.-J. Morcrette, B.-K. Park, C. Peubey, P. de Rosnay, C. Tavolato, J.-N. Thepaut, and F. Vitart (2011), The ERA-Interim reanalysis: configuration and performance of the data assimilation system, *Quart. J. Roy. Meteor. Soc*, *137*, 553–597.

Dima, I. M., and J. M. Wallace (2003), On the seasonality of the Hadley cell, *J. Atmos. Sci.*, *60*, 1522–1527.

Emanuel, K. A., J. D. Neelin, and C. S. Bretherton (1994), On large-scale circulations in convecting atmospheres, *Quart. J. Roy. Meteor. Soc.*, *120*, 1111–1143.

Gill, A. E. (1980), Some simple solutions for heat-induced tropical circulation, *Quart. J. Roy. Meteor. Soc.*, *106*, 447–462.

Gill, A. E. (1982), *Atmosphere-Ocean Dynamics*, *International Geophysics Series*, vol. 30, 662 pp., Academic Press.

Gonzalez, A. O., C. J. Slocum, R. K. Taft, and W. H. Schubert (2016), Dynamics of the itcz boundary layer, *Journal of the Atmospheric Sciences*, *73*(4), 1577–1592, doi:10.1175/JAS-D-15-0298.1.

Green, B., and J. Marshall (2017), Coupling of trade winds with ocean circulation damps itcz shifts, *J. Climate*, *30*, 4395–4411, doi:10.1175/JCLI-D-16-0818.1.

Gu, G., R. Adler, and A. Sobel (2005), The eastern Pacific ITCZ during the boreal spring, *J. Atmos. Sci.*, *62*, 1157–1174.

Haffke, C., G. Magnusdottir, D. Henke, P. Smyth, and Y. Peings (2016), Daily states of the March-April east Pacific ITCZ in three decades of high-resolution satellite data, *J. Climate*, *29*, 2981–2995.

Held, I. M., and B. J. Soden (2006), Robust responses of the hydrological cycle to global warming, *J. Climate*, *19*, 5686–5699.

Holton, J. R., and D. E. Colton (1972), A diagnostic study of the vorticity balance at 200 mb in the tropics during the northern summer, *J. Atmos. Sci.*, *29*, 1124–1128.

Holton, J. R., J. M. Wallace, and J. A. Young (1971), On boundary layer dynamics and the itcz, *Journal of the Atmospheric Sciences*, *28*(2), 275–280.

Karnauskas, K. B., R. Seager, A. Kaplan, Y. Kushnir, and M. Cane (2009), Observed strengthening of the zonal sea surface temperature gradient across the equatorial Pacific ocean, *J. Climate*, *22*, 4316–4321, doi:10.1175/2009JCLI2936.1.

Krishnamurti, T. N. (1971a), Observational study of the tropical upper troposphere motion field during the northern hemisphere summer, *J. Appl. Meteor.*, *10*, 1066–1096.

Krishnamurti, T. N. (1971b), Tropical east-west circulations during the northern summer, *J. Atmos. Sci.*, *28*, 1342–1347.

Lin, J.-L. (2007), The double-ITCZ problem in IPCC AR4 coupled GCMs: Ocean–atmosphere feedback analysis, *J. Climate*, *20*, 4497–4525.

Lin, J. L., B. E. Mapes, and W. Han (2008), What are the sources of mechanical damping in matsuno–gill-type models?, *J. Climate*, *21*, 165–179.

Lindzen, R. S., and S. Nigam (1987), On the role of sea surface temperature gradients in forcing low-level winds and convergence in the Tropics, *J. Atmos. Sci.*, *44*, 2418–2436.

Matsuno, T. (1966), Quasi-geostrophic motions in the equatorial area, *J. Meteor. Soc. Japan*, *44*, 25–42.

McGauley, M., C. Zhang, and N. A. Bond (2004), Large-scale characteristics of the atmospheric boundary layer in the eastern pacific cold tongue-ITCZ region, *Journal of Climate*, *17*(20), 3907–3920, doi:10.1175/1520-0442(2004)017¡3907:LCOTAB¿2.0.CO;2.

Möbis, B., and B. Stevens (2012), Factors controlling the position of the intertropical convergence zone on an aquaplanet, *J. Adv. Model. Earth Syst.*, *4*, M00A04, doi:10.1029/2012MS000199.

Neelin, J. D. (1989), On the interpretation of the Gill model, *J. Atmos. Sci.*, *46*, 2466–2468.

Neelin, J. D. (2011), *Climate Change and Climate Modeling*, 293 pp., Cambridge Univ. Press.

Ooyama, K. V. (1982), Conceptual evolution of the theory and modeling of the tropical cyclone, *Journal of the Meteorological Society of Japan*, *60*, 369–379.

Oueslati, B., and G. Bellon (2015), The double ITCZ bias in CMIP5 models: interaction between SST, large-scale circulation and precipitation, *Clim. Dyn.*, *44*, 585–607.

Raymond, D., Z. Fuchs, S. Gjorgjievska, and S. Sessions (2015), Balanced dynamics and convection in the tropical troposphere, *J. Adv. Model. Earth Sys.*, *7*, doi:10.1002/ 2015MS000467.

Raymond, D. J., C. S. Bretherton, and J. Molinari (2006), Dynamics of the intertropical convergence zone of the east pacific, *Journal of the Atmospheric Sciences*, *63*(2), 582–597, doi:10.1175/JAS3642.1.

Romps, D. M. (2014), Rayleigh damping in the free troposphere, *J. Atmos. Sci.*, *71*, 553–565.

Sardeshmukh, P. D., and I. M. Held (1984), The vorticity balance in the tropical upper troposphere of a general circulation model, *J. Atmos. Sci.*, *41*, 768–778.

Schneider, T., and S. Bordoni (2008), Eddy-mediated regime transitions in the seasonal cycle of a Hadley circulation and implications for monsoon dynamics, *J. Atmos. Sci.*, *65*, 915–934.

Schneider, T., T. Bischoff, and G. H. Haug (2014), Migrations and dynamics of the intertropical convergence zone, *Nature*, *513*, 45–53, doi:10.1038/nature13636.

Smith, T., R. Reynolds, T. Peterson, and J. Lawrimore (2008), Improvements to NOAA's historical merged land-ocean surface temperature analysis (1880-2006), *J. Climate*, *21*, 2283–2296.

Sobel, A. H., and J. D. Neelin (2006), The boundary layer contribution to Intertropical Convergence Zones in the quasi-equilibrium tropical circulation model framework, *Theor. Comput. Fluid Dyn.*, *20*, 323–350.

Stommel, H. (1948), The westward intensification of wind-driven ocean currents, *Eos, Transactions American Geophysical Union*, *29*(2), 202–206, doi:10.1029/TR029i002p00202.

Trenberth, K. E., and D. J. Shea (2005), Relationships between precipitation and surface temperature, *Geophysical Research Letters*, *32*(14), n/a–n/a, doi:10.1029/2005GL022760, l14703.

van der Wiel, K., A. J. Matthews, D. P. Stevens, and M. M. Joshi (2015), A dynamical framework for the origin of the diagonal South Pacific and South Atlantic convergence zones, *Quart. J. Roy. Meteor. Soc.*, *141*(691), 1997–2010, doi:10.1002/qj.2508.

van der Wiel, K., A. J. Matthews, and D. P. Stevens (2016), Why the South Pacific Convergence Zone is diagonal, *Clim. Dyn.*, *46*(5), 1683–1698, doi:10.1007/s00382-015-2668-0.

Vincent, E. M., M. Lengaigne, C. E. Menkes, N. C. Jourdain, P. Marchesiello, and G. Madec (2011), Interannual variability of the south pacific convergence zone and implications for tropical cyclone genesis, *Climate Dynamics*, *36*(9), 1881–1896, doi:10.1007/s00382-009-0716-3.

Voigt, A., and T. A. Shaw (2015), Circulation response to warming shaped by radiative changes of clouds and water vapour, *Nature Geosci.*, *8*, 102–106, doi:10.1038/NGEO2345.

Waliser, D. E., and R. C. J. Somerville (1994), Preferred latitudes of the intertropical convergence zone, *J. Atmos. Sci.*, *51*, 1619–1639.

Widlansky, M. J., P. J. Webster, and C. D. Hoyos (2011), On the location and orientation of the south pacific convergence zone, *Climate Dynamics*, *36*(3), 561–578, doi:10.1007/s00382-010-0871-6.

Xie, S.-P. (2004), The shape of continents, air-sea interaction, and the rising branch of the Hadley circulation, in *The Hadley Circulation: Present, Past and Future*, *Advances in Global Change Research*, vol. 21, edited by H. F. Diaz and R. S. Bradley, pp. 121–152, Kluwer Academic Publishers, Dordrecht, Netherlands.

Zhang, C. (2001), Double ITCZs, *J. Geophys. Res.*, *106*, 785–11 792.

Corresponding author: Ori Adam, The Fredy & Nadine Herrmann Institute of Earth Sciences The Hebrew University, Jerusalem 9190401, Israel. (ori.adam@mail.huji.ac.il)